

# Individual variability in functional connectivity predicts performance of a perceptual task

Antonello Baldassarre<sup>a,b,1</sup>, Christopher M. Lewis<sup>a,b,c,1</sup>, Giorgia Committeri<sup>a,b</sup>, Abraham Z. Snyder<sup>d</sup>, Gian Luca Romani<sup>a,b</sup>, and Maurizio Corbetta<sup>a,b,d,e,2</sup>

<sup>a</sup>Institute for Advanced Biomedical Technologies, Foundation G. d'Annunzio, Chieti 66100, Italy; <sup>b</sup>Department of Neuroscience and Imaging, University of Chieti G. d'Annunzio, Chieti 66100, Italy; <sup>c</sup>Ernst Strüngmann Institute in Cooperation with Max Planck Society, 60528 Frankfurt am Main, Germany; <sup>d</sup>Department of Radiology, Washington University School of Medicine, St. Louis, MO 63110; and <sup>e</sup>Departments of Neurology, Anatomy, and Neurobiology, Washington University School of Medicine, St. Louis, MO 63110

Edited by Michael Posner, University of Oregon, Eugene, OR, and approved December 30, 2011 (received for review August 15, 2011)

People differ in their ability to perform novel perceptual tasks, both during initial exposure and in the rate of improvement with practice. It is also known that regions of the brain recruited by particular tasks change their activity during learning. Here we investigate neural signals predictive of individual variability in performance. We used resting-state functional MRI to assess functional connectivity before training on a novel visual discrimination task. Subsequent task performance was related to functional connectivity measures within portions of visual cortex and between visual cortex and prefrontal association areas. Our results indicate that individual differences in performing novel perceptual tasks can be related to individual differences in spontaneous cortical activity.

predisposition | visual learning | spontaneous activity

Healthy observers differ in their ability to perform a variety of visual tasks (1). Individuals also differ in their ability to improve with training (2–6), i.e., perceptual learning (7, 8). Initial performance and rate of learning tend to be inversely related (3, 9). Thus, individuals who perform better initially tend to exhibit slower improvement. Although the physiological correlates of perceptual learning have been well documented at the level of individual synapses (10), neurons (11, 12), and large-scale networks (6, 13–16), it is largely unknown whether the state of the brain before training influences future performance or the rate of acquisition of a novel task. Here we investigate the extent to which performance of a novel perceptual task can be predicted on the basis of physiological measures evaluated before training. Our measure of performance takes into account both early and late features of the psychophysical learning curve.

Intrinsic neural activity is temporally correlated within widely distributed networks that recapitulate the topography of task-related functional responses (17–21). Hence, resting-state functional connectivity offers a plausible neural correlate of behavioral predisposition to perform a novel task. Moreover, resting-state measures have been correlated with individual performance variability in several cognitive domains (22–26). However, to our knowledge, no study to date has shown that functional connectivity, measured before training, within cortical circuits later recruited by a novel task, is predictive of future performance.

In previous work (15), we showed that resting-state blood oxygenation level-dependent signal functional connectivity (FC) changes in task-relevant cortical networks after extensive practice on a novel orientation discrimination task. Critically, post-learning modulations in FC correlated with individual measures of improvement.

Here, we analyze the same dataset to test the hypothesis that FC in task-relevant circuits, measured before training, is predictive of subsequent performance.

## Results

**Behavior.** Healthy observers ( $n = 14$ , seven male) were trained to report the presence/absence of a target shape (an inverted letter

T) (14) always presented in the lower left visual quadrant (15) (Fig. 1A, *Methods*, and *SI Methods*). Targets and distractors (letter Ts of different orientation) were presented together in a circular array at 5° of eccentricity. The criterion for successful acquisition of the task was a normalized accuracy equal to or greater than 80% over 10 consecutive blocks of trials, with each block including 45 trials (14, 15, 27):

$$\text{Normalized accuracy} = (\text{hits} [\%] + \text{correct rejections} [\%]) - \text{false alarms} [\%] / 1 - \text{false alarms} [\%] \quad [1]$$

On average, observers took approximately 5,600 trials or 118 blocks (~4 d of 2–3 h practice per day) to reach the criterion (Fig. 1B). We observed a high degree of individual variability at the beginning of training. Accuracy on the first 10 blocks, the minimum number of blocks performed on the first day, was 41% with large interindividual variability (range, 13–69%). Psychophysical performance curves were fit by using the following empirical two-parameter expression:

$$a = a_0 + s \log(k) \quad [2]$$

where  $a$  is accuracy,  $k$  indexes block,  $a_0$  is initial accuracy on the first block, and  $s$  is a scaling parameter numerically equal to the initial slope. Fits of the analytic expression to the individual performance data were expressed in terms of variance explained ( $r^2$ ): median  $r^2$  was 0.68, with a range of 0.29 to 0.93 (Fig. 1B and Fig. S1). In addition to  $a_0$  and  $s$ , we evaluated the number blocks needed to achieve the criterion (performance  $\geq 80\%$ ;  $k_c$ ). The three measures were correlated (*SI Methods* and Fig. S2) in a manner consistent with previous studies of perceptual learning (3, 9). Thus, subjects with high initial accuracy learned the task in fewer blocks but at a lower rate of improvement. Conversely, subjects with lower initial accuracy took longer to reach criterion but their rate of improvement was higher. Because of these relations and the relatively small size of the study group, it was not possible to derive independent measures of initial performance and rate of learning. To obtain individual quantitative indices of performance,  $a_0$ ,  $s$ , and  $k_c$  were entered into a principal component analysis (Fig. S3). The first component (PC1) explained 75% of the variance. The second component accounted for 15% of the

Author contributions: A.B., C.M.L., G.C., and M.C. designed research; A.B., C.M.L., and M.C. performed research; A.B., C.M.L., and A.Z.S. analyzed data; and A.B., C.M.L., G.C., A.Z.S., G.L.R., and M.C. wrote the paper.

The authors declare no conflict of interest.

This article is a PNAS Direct Submission.

<sup>1</sup>A.B. and C.M.L. equally contributed to this work.

<sup>2</sup>To whom correspondence should be addressed. E-mail: mau@npg.wustl.edu.

This article contains supporting information online at [www.pnas.org/lookup/suppl/doi:10.1073/pnas.1113148109/-DCSupplemental](http://www.pnas.org/lookup/suppl/doi:10.1073/pnas.1113148109/-DCSupplemental).

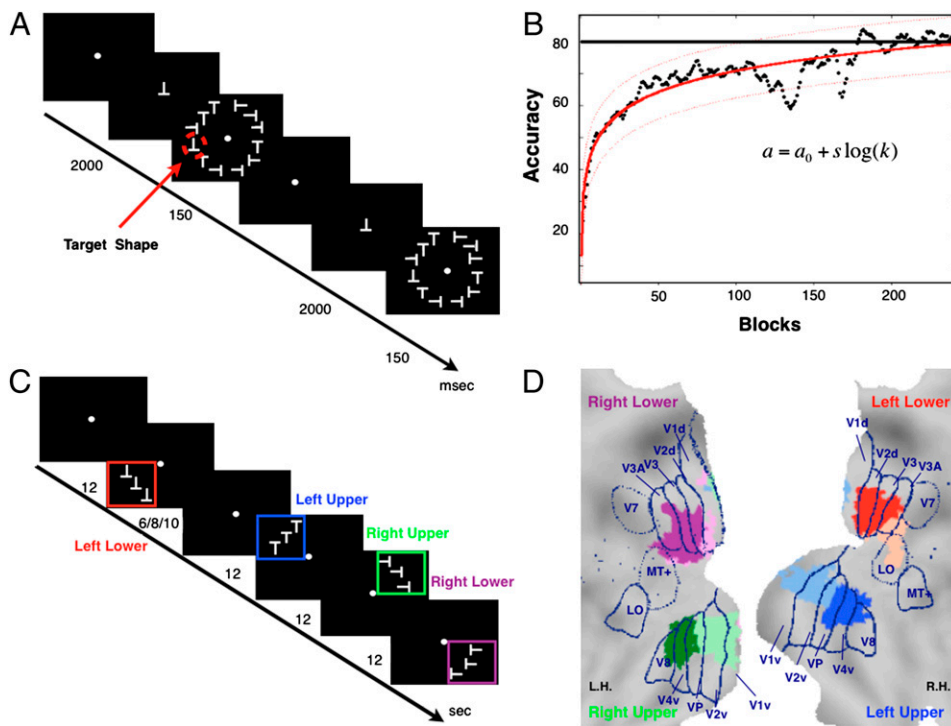


**Fig. 1.** Behavioral training, psychophysics results, visuotopic localizer, and ROIs. (A) Experimental paradigm. (B)  $x$  axis, number of blocks;  $y$  axis, accuracy (i.e., percentage of correct response corrected for percentage of false alarms). Black dots display the group average performance block by block; solid red line indicates the psychophysical fitting model  $a = a_0 + s \log(k)$  with prediction bounds at 95% of confidence level (dotted lines). (C) Design of visuotopic localizer. Squares of different colors (not shown in real display) indicate a visual quadrant. (D) Visual ROIs/seeds. Eight visual regions (seeds) defined on the basis of the visuotopic localizer scan are displayed on the flattened representation of posterior occipital cortex using the PALS atlas (29). Blue lines are approximate borders between retinotopic visual areas based on a standard atlas (29) L.H., left hemisphere; R.H., right hemisphere.

variance, but its eigenvalue was less than 1 (scree plot in Fig. S3) and it was therefore not further considered (28). Accordingly, PC1 was used to compute individual measures of performance, which we here define as task fitness ( $f$ ) by using the following expression:

$$f = [a_0 \ s \ k_c] \cdot w \quad [3]$$

where  $w$  is the vector of factor weights (SI Methods). In the rest of the analysis, we use task fitness to examine the relationship between performance and pretraining resting-state FC.

**Pretraining FC in Visual Cortex and Task Fitness.** Resting-state functional MRI (fMRI) and visuotopic localizer fMRI were acquired 24 to 48 h before first exposure to the task (Methods and SI Methods). During the visuotopic localizer scans, subjects were asked to maintain central fixation while quarter-field stimulus arrays were passively presented in a blocked design (Fig. 1C). Regions of interest (ROIs) for the computation of FC were identified in the ventral and dorsal portions of visual cortex in each hemisphere. At the group level, two ROIs were identified in each quadrant as showing the strongest visuotopic localizer responses (e.g., in right dorsal cortex for left lower field stimulation) compared with the average response to stimuli in the other quadrants [group-level voxel-wise random-effect ANOVAs, multiple comparison corrected over the entire brain ( $P < 0.05$ )]. These regions are shown in Fig. 1D on a flattened representation of visual cortex in the Population Average Landmark and Surface (PALS) atlas (29) and labeled according to their location with respect to the probabilistic borders of visual areas in the same atlas (Table S1). In general, for each quarter-field representation in visual cortex, one ROI is “early” in the visual hierarchy (near/at V1–V2), whereas the other is “intermediate” (near/at V4–V8 or V3A; Fig. 1D; Table S1 shows coordinates).

To examine the relationship between pretraining FC and the ability to perform the discrimination task, we computed group-level voxel-wise maps of the Pearson correlation coefficient between task fitness and the strength of FC for each visuotopic

ROI (defined as FC–PC1 correlation maps; Methods, SI Methods, and Fig. S4). Fig. 2A shows that the strength of FC between a representative ROI in right ventral visual cortex (near/at V1–V2) and large swaths of ventral and dorsal peripheral visual cortex in both hemispheres is strongly correlated with task fitness (all voxels  $Z > 2$ ;  $P < 0.05$ , Monte Carlo corrected). Observers with stronger pretraining FC between visual regions displayed greater task fitness (Fig. 2B). This relationship was consistent across different ROIs in left and right visual cortex (Fig. S5). To quantify this consistency, a conjunction map was computed that shows the portions of visual cortex with behaviorally predictive FC across multiple ROIs (Fig. 2C). The most consistent regions encompassed both early and intermediate retinotopic areas, including a band outside the foveal region in the near periphery (based on the PALS borders).

To examine whether the regions exhibiting behaviorally significant pretraining FC coded for the stimuli, we quantified the percentage of voxels in the FC–PC1 conjunction map that overlapped with the regions in visual cortex selectively activated by the stimulus array (i.e., the sum of the quadrant maps). At a threshold of four of eight ROIs, 72% of the behaviorally predictive voxels from the FC–PC1 conjunction map fell within the borders of the region activated by the stimulus (Fig. 2D). This proportion increased to 86% when the threshold was increased to five of eight ROIs.

Computing pairwise correlations for all ROIs and calculating the correlation with task fitness confirmed these findings. The range of FC–PC1 correlations varied between an  $r$  of 0.1 and an  $r$  of 0.8; 13 of 28 (or  $8 \times 7/2$ ) possible ROI pairs showed a significant correlation with task fitness [false discovery rate (FDR),  $q < 0.05$  after random permutation test]. Thus, voxel-wise and regional analyses confirmed a significant relationship between task fitness and pretraining FC in portions of visual cortex activated by the visuotopic localizer stimuli. Fig. 3A shows the group average strength of FC between ROI pairs arranged by visual quadrant (i.e., dorsal, ventral). Fig. 3B shows behaviorally significant FC. Behaviorally predictive correlations (FC–PC1) were observed predominantly in heterotopic region pairs, i.e., region pairs in different quadrants within the same (e.g., left dorsal to ventral

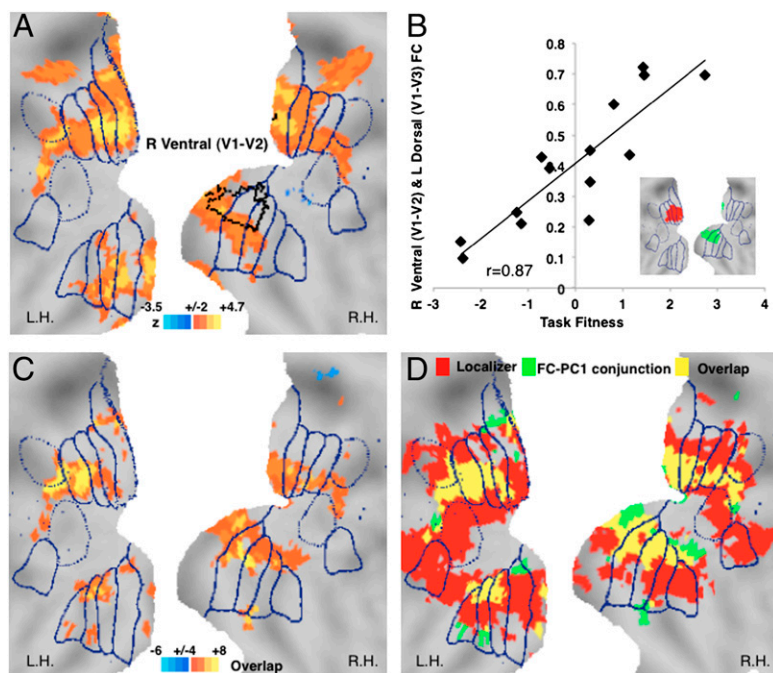


**Fig. 2.** Task fitness and pretraining FC to/from visual cortex. (A) Voxel-wise FC-PC1 correlation map starting from a seed region in the right ventral visual seed (V1-V2; black border), corresponding to the left upper visual quadrant. The map is projected onto a flattened representation of the posterior occipital cortex using the PALS atlas (29). Color scale: yellow/orange indicates positive correlation (Z-statistic of Pearson  $r$ ) thresholded at  $Z > 2$ ,  $P < 0.05$ , and Monte Carlo corrected. Blue color indicates negative correlation. Blue lines are the same as in Fig. 1D. L.H., left hemisphere; R.H., right hemisphere. (B) x axis, task fitness, i.e., principal component scores of PC1; y axis, FC (Fisher Z-transformed) between a right ventral visual seed V1-V2 (green, *inset*; same as in A) and a left dorsal visual region (red) extracted from the FC-PC1 correlation map in A (Talairach coordinates,  $-06 -96 +08$ ; 185 voxels). Each diamond represents an observer. (C) Conjunction of eight voxel-wise FC-PC1 correlation maps, one for each visual seed shown in Fig. 1D (Table S1 provides coordinates). Color scale: yellow/orange indicates overlap of positive correlations (range, 1-8); cyan/blue indicates overlap of negative correlations. (D) Conjunction map between visuotopic localizer activations (Z-statistic  $> 3$ ,  $P < 0.05$ , Monte Carlo corrected; *Methods*; red) and FC-PC1 conjunction map thresholded four of eight (green). Overlapped voxels are in yellow.

cortex) or different hemispheres (e.g., left dorsal to right ventral cortex; Fig. 3 B and C), rather than homotopic region pairs (e.g., right dorsal to left dorsal cortex; Fig. 3 B and D) or local connectivity (e.g., right dorsal V1-V3 to right dorsal V3A-LO; permutation test on the entire correlation matrix, FDR  $q < 0.05$ ; Fig. 3 B and E).

**Pretraining FC Between Visual and Frontoparietal Regions and Task Fitness.** Behaviorally predictive FC with visuotopic areas extended also to a small number of regions in higher-order frontal and posterior parietal cortex (Fig. S64). Fig. 4A shows FC between a right dorsal visual ROI and left anterior insula, belonging to the “control network” (30, 31), which was negatively correlated with task fitness. Observers who performed better on the orientation discrimination task tended to have stronger negative correlation (i.e., antiphase coherence) between spontaneous activity in visual cortex and anterior insula (Fig. 4B). This result is representative of multiple visual ROIs (four of eight visual ROIs; Fig. 4C). Interestingly, this region overlaps with an insular region activated by the orientation discrimination task (Fig. 4D and *SI Methods*). A similar pattern was detected in the right medial prefrontal cortex, a part of the default mode network (32, 33) (Fig. 4 E-H). Again, more negative FC corresponded to greater task fitness (Fig. 4F). This region overlaps with a larger medial prefrontal region deactivated by task performance (Fig. 4H and *SI Methods*). Similar negative FC-PC1 correlations, i.e., more negative FC corresponding to better performance, were detected in other default mode regions, in left middle temporal cortex and right/left angular gyrus (Fig. S64 and Table S2). All regions in higher-order cortex that showed predictive FC with visual cortex overlapped regions recruited by the orientation discrimination task (Fig. S6 B and C), albeit in a small proportion of the total extent of cortex recruited by the task.

**Control Analyses: Auditory Cortex.** To examine the modality specificity of these effects, and rule out the possibility that FC-performance correlations merely reflected a high level of FC in neighboring areas, a set of control analyses was run on primary and secondary auditory regions (*SI Methods*; Table S1 shows coordinates). The auditory regions were selected based on two criteria: anatomical location and task deactivation during the

orientation discrimination task. In fact, primary and secondary auditory regions are typically deactivated during visual tasks (32). From the auditory regions, we computed baseline FC and FC-PC1 correlation maps, which were compared with the visual regions. Both neighboring visual (Fig. S7A) and auditory regions (Fig. S7C) showed strong FC. However, auditory regions (Fig. S7D), in contrast to visual regions (Fig. S7B), did not show a predictive relationship with task fitness. We conclude that the behaviorally predictive pretraining FC is modality specific, and is not driven by local connectivity.

## Discussion

We show that certain patterns of resting state FC within visual cortex, and between visual cortex and higher-order cortical regions, represent neural predictors of observer predisposition to perform a novel orientation discrimination task. Several previous studies have reported correlations between performance measures and fMRI FC (22-26). However, this study, as far as we are aware, is the first to demonstrate that FC, before any exposure, is predictive of performance and acquisition on a novel task. In addition, its topography coincides with the areas subsequently recruited by task performance.

**Task Fitness: Initial Performance, Rate, and Duration of Learning.** The behavioral component identified by the factor analysis (i.e., PC1) combined aspects of initial performance (i.e., predisposition), the rate of performance improvement, and the quantity of practice required to reach criterion. Our observers were highly variable in their initial performance, a finding concordant with previous studies of complex visual tasks (1) as well as perceptual learning (2-4, 6). Interestingly, task fitness was positively correlated with initial performance, and negatively correlated with the rate of learning and the number of blocks to criterion. Hence, subjects with high initial performance reached criterion earlier but at a slower rate, consistent with early reports on perceptual learning (3, 9). Our results therefore suggest that the state of the system at the beginning of training may influence the way the observers learn when the task requires extensive cortical processing.

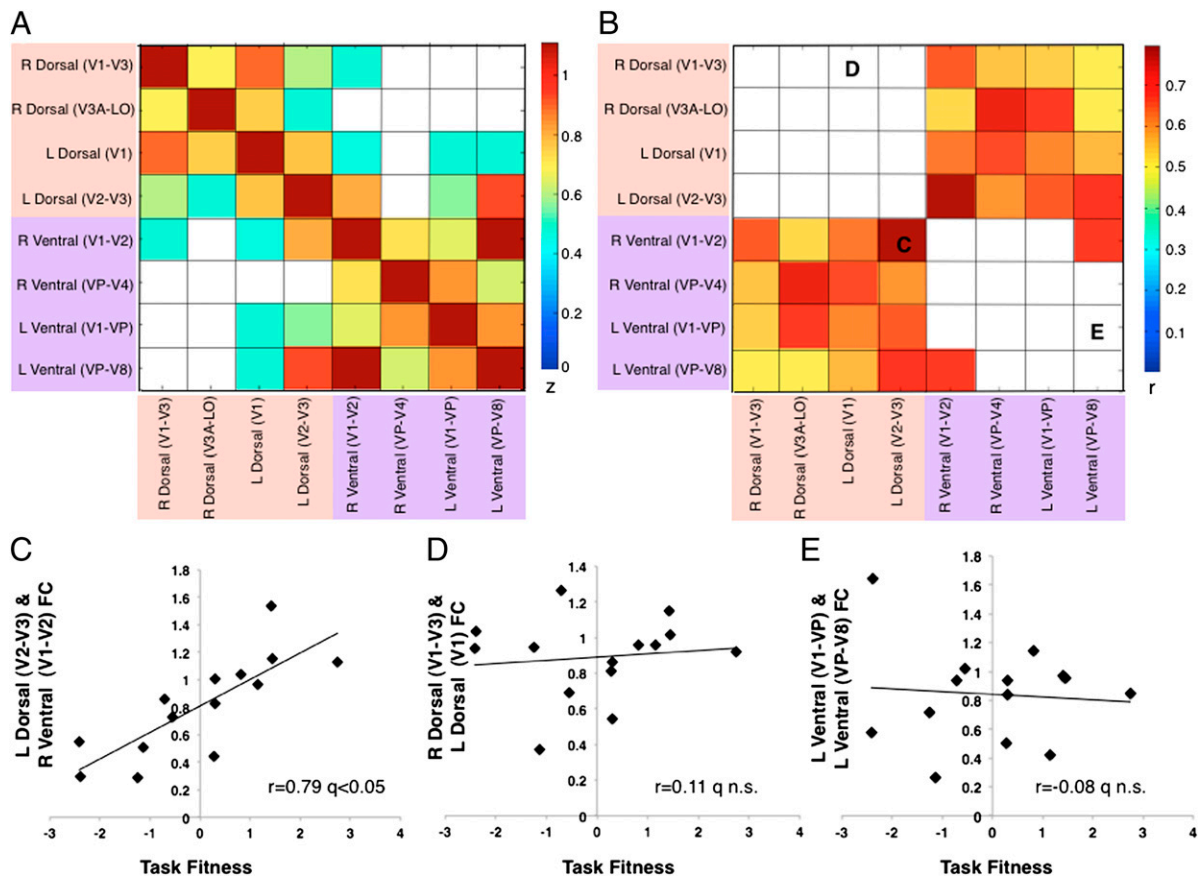


**Fig. 3.** Task fitness and pretraining FC within visual cortex. (A) Correlation matrix (Fisher Z-transformed Pearson coefficient) of all ROI pairs in visual cortex. Yellow/orange color indicates positive correlations, white color indicates nonsignificant correlations (permutation test on the entire correlation matrix; FDR  $q < 0.05$ ). Dorsal visual regions are highlighted by light pink, ventral visual regions by light purple. (B) Correlation matrix (Pearson coefficient  $r$ ) of PC1 and FC between all possible ROI pairs in visual cortex. Red/yellow cells indicate positive FC-PC1 correlations, white cells indicate nonsignificant correlations (permutation test on the entire correlation matrix; FDR  $q < 0.05$ ). (C-E) x axis, task fitness, i.e., principal component scores of PC1; y axis, FC (Fisher Z-transformed) between two heterotopic (C), homotopic (D), and neighboring (E) visual regions. Each diamond represents an observer. For Pearson correlation coefficient, permutation test was performed on the entire correlation matrix (FDR  $q < 0.05$ ).

**Predictive Intrinsic FC.** Predictive FC was observed in region pairs including visual cortex as well as prefrontal and insular areas involved in cognitive control. All predictive regions were a subset of the cortical regions driven by the orientation discrimination task. Two patterns of FC were predictive of task fitness. In visual cortex, observers with stronger heterotopic functional connections, i.e., linking cortex representing dorsal and ventral quadrants within or between hemispheres, exhibited higher task fitness. In contrast, the strength of homotopic connections, i.e., linking dorsal or ventral quadrants across hemispheres, or of local connections, i.e., linking adjacent regions in visual cortex, was not predictive of performance. This result is noteworthy because local and homotopic FC typically is stronger than heterotopic FC (34, 35).

A possible interpretation is that heterotopic connections linking different quadrants in visual cortex are more important for the dynamic reweighting of functional connections that occur in the course of learning. The orientation discrimination task required subjects to direct spatial attention to the left lower quadrant. Important processes for acquisition of the task include filtering of distracters at multiple unattended locations (36), as well as coding of the locus of attention by gradients of activity across spatial maps (37, 38). Hence, a high degree of coherence between stimulus-specific regions in visual cortex, before any experience, may facilitate the subsequent parsing of relevant from irrelevant information, and facilitate the reweighting of functional connections among different quadrants in visual

cortex. At the end of learning, in agreement with this hypothesis, stronger responses to target shapes were recorded only in the trained visual quadrant, and FC was differentially modulated in trained and untrained quadrants (15).

The second predictive pattern of FC was an inverse correlation between spontaneous activity in visual cortex and regions of the default mode (32, 33) and control (30) networks. This finding is also consistent with learning-related changes reported in our previous study (15), and in the work of Sigman et al. (14). We previously found that FC between unattended quadrants in visual cortex and default mode regions decreased (i.e., became less negative) after learning, and that these decrements correlated with measures of perceptual learning. Sigman et al. reported that decreases in task-evoked deactivation in the default mode network correlated with learning on the same task (14). Observers with stronger negative correlation between visual cortex and default mode regions at baseline may find it easier to filter out distracters at unattended locations early in training, which becomes less important as target selection becomes more automatic. This interpretation is consistent with a role of the default mode network in filtering out unattended stimuli, as suggested by other studies (39–41). Behaviorally significant negative correlations in FC between visual cortex and default mode regions have also been reported in relation to reading skills in children and adults, a competency closely related to orientation discrimination (25).

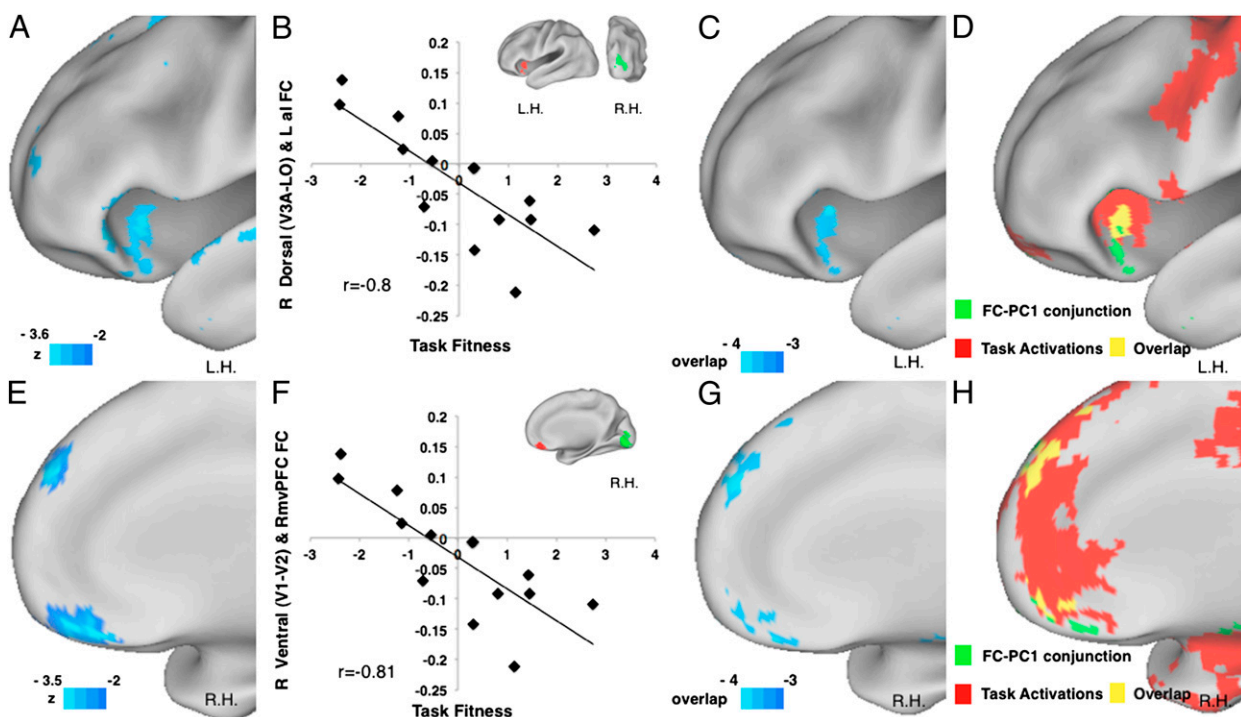


**Fig. 4.** Task fitness and pretraining FC to/from visual cortex and frontal regions. (A) Lateral view of the voxel-wise FC–PC1 correlation map starting from a right dorsal visual seed (V3A–LO), corresponding to the left lower visual quadrant. Color scale is the same as in Fig. 2. L.H., left hemisphere. (B) x axis, task fitness; y axis, FC (Fisher Z-transformed) between a right dorsal visual seed V3A–LO (green, *Inset*; same as in A) and left anterior insula (LAI; red) extracted from the FC–PC1 correlation map in A (Talairach coordinates,  $-38 +18 -07$ ; 171 voxels). Each diamond represents an observer. (C) Conjunction map of FC–PC1 correlation maps from eight visual seeds. Color scale is the same as in Fig. 2. (D) Conjunction map between activation map of orientation discrimination task (trained plus untrained shape greater than fixation, Z-statistic  $>3$ ,  $P < 0.05$ , Monte Carlo corrected; *Methods*) and FC–PC1 conjunction map thresholded at negative three of eight (green). Overlapped voxels are in yellow. (E) Medial view of the voxel-wise FC–PC1 correlation map starting from a right ventral visual seed (V1–V2), corresponding to the left upper visual quadrant. Color scale is the same as in A. R.H., right hemisphere. (F) x axis as in B; y axis is FC (Fisher Z-transformed) between a right ventral visual seed V1–V2 (green, *Inset*) and a right ventral medial prefrontal cortex (RvmPFC; red) extracted from the FC–PC1 correlation map in A (Talairach coordinates,  $+04 +38 -18$ ; 120 voxels). Each diamond represents an observer. (G) Medial view of the same conjunction map in B, with the same color scale. (H) Conjunction map between deactivation map of orientation discrimination task (trained plus untrained shape less than fixation, Z-statistic  $>3$ ,  $P < 0.05$ , Monte Carlo corrected; *Methods*) and FC–PC1 conjunction map thresholded negative three of eight (green). Overlapped voxels are in yellow.

**Putative Underlying Mechanisms.** One possible substrate for the predictive relationship between task fitness and FC is individual variability in structural connectivity. The strength of structural connections has been correlated with the strength of FC at the level of both large-scale networks (42) and local microcircuitry (43), and has also been shown to exhibit experience-dependent plasticity (44). However, in our study, regions exhibiting predictive FC (i.e., heterotopic connections in visual cortex, and visual, default, and control) showed weaker baseline FC. The logical inference would be that these areas are less well anatomically connected (42). Moreover, in primate studies, subdivisions of visual cortex with behaviorally predictive (i.e., heterotopic) functional coupling tend to have weaker anatomical connectivity than nonpredictive (i.e., homotopic) regions (45).

Another mechanism that could be related to our results is the recent observation that fMRI FC is related to slow cortical potentials and band-limited fluctuations of power in higher frequencies (46–48). These relatively slow fluctuations in neural excitability may facilitate synchronization of high-frequency activity through a variety of mechanisms (49, 50), and enable the coordination of task-relevant circuits. This could explain why observers with stronger FC within visual cortex, or between visual and other task-relevant areas in prefrontal and insular cortex, can recruit those regions more efficiently when performing a novel task.

We conclude that individual variability of FC within visual cortex, and between visual and higher-order regions, is related to the predisposition to perform a novel visual discrimination task.

These findings suggest a potential role of intrinsic brain activity as a neural predictor of perceptual skill acquisition. This result has general implications for the functional significance of spontaneous activity, and the neural bases of individual behavioral variability. In addition, our findings emphasize the importance of spontaneous activity, and the state of FC, as a possible “neural” prior for biasing task-evoked activity and behavior (51–53).

## Methods

**Participants.** Healthy right-handed observers ( $N = 14$ ) provided written informed consent approved by the Research Ethics Board of the University of Chieti.

**Behavioral Training.** Observers were instructed to attend to the left lower visual quadrant and report with a key press the presence/absence of a target shape (an inverted letter T) in a briefly presented radial display of randomly oriented letter-T distracters. Central fixation was monitored with an eye tracker. Criterion for learning was 10 blocks of trials with accuracy of at least 80%.

**fMRI Scanning.** Functional images (gradient-echo sequence, repetition time of 2.163 s, echo time of 50 ms, flip angle  $90^\circ$ , slice thickness of 8 mm,  $3.75 \times 3.75$  mm in-plane resolution) were acquired during passive stimulation of each visual quadrant with the same display used for perceptual learning (i.e., localizer). Localizer scans were used to define ROIs/seeds for the FC analysis of resting-state data obtained before any exposure to the task.

**Behavioral Score.** Task fitness was defined as the first factor (i.e., PC1) of a principal component analysis on the parameters of a natural logarithmic function, plus the number of blocks to criterion, used to quantify observer learning curves. This component accounted for 75% of the behavioral

variance and was correlated with initial performance, rate of learning, and number of blocks to criterion.

**FC–PC1 Correlation.** Voxel-wise or ROI pair FC–PC1 correlations were computed as the Pearson correlation coefficient  $r$  between FC measures and task fitness (*Results*). FC was conventionally computed as the Pearson correlation between the time series extracted from a predefined ROI (e.g., left ventral visual cortex) and the rest of the brain (to obtain voxel-wise maps) or another ROI (to obtain ROI–ROI FC; *SI Methods* provides detailed information). Voxel-wise statistical significance in correlation maps was evaluated by first expressing the result as equi-probable Z score maps, which were then corrected for multiple comparisons. Significance thresholds for ROI pair FC were

computed by permutation simulations. Presently reported ROI pair results are FDR corrected with a  $q$ -value lower than 0.05.

**ACKNOWLEDGMENTS.** We thank Drs. Annalisa Tosoni and Valentina Sebastiani for data collection; Dr. Francesco de Pasquale for discussion on data analysis; Dr. Gordon Shulman for reading and commenting on a draft of the manuscript; Dr. Mariano Sigman, one of the reviewers, for suggesting the principal component analysis on the behavioral data; and the other anonymous reviewer for constructive criticisms on the earlier draft. This work was supported by European Union (EU) Grants FP6-MEXC-CT-2004–006783 (Ibsen) and FP7 200728 (Brain-Synch), National Institute of Mental Health Grant 1R01MH096482, National Institutes of Health Grant NS48013, and the Third PhD Internationalization Program of the Italian Ministry of University and Research.

- Halpern SD, Andrews TJ, Purves D (1999) Interindividual variation in human visual performance. *J Cogn Neurosci* 11:521–534.
- Fahle M, Edelman S, Poggio T (1995) Fast perceptual learning in hyperacuity. *Vision Res* 35:3003–3013.
- Fahle M, Henke-Fahle S (1996) Interobserver variance in perceptual performance and learning. *Invest Ophthalmol Vis Sci* 37:869–877.
- Schmitt C, Kromeier M, Bach M, Kommerell G (2002) Interindividual variability of learning in stereoacuity. *Graefes Arch Clin Exp Ophthalmol* 240:704–709.
- Fahle M (2004) Perceptual learning: A case for early selection. *J Vis* 4:879–890.
- Mukai I, et al. (2007) Activations in visual and attention-related areas predict and correlate with the degree of perceptual learning. *J Neurosci* 27:11401–11411.
- Gilbert CD, Sigman M, Crist RE (2001) The neural basis of perceptual learning. *Neuron* 31:681–697.
- Sasaki Y, Nanez JE, Watanabe T (2010) Advances in visual perceptual learning and plasticity. *Nat Rev Neurosci* 11:53–60.
- Fahle M (1997) Specificity of learning curvature, orientation, and vernier discriminations. *Vision Res* 37:1885–1895.
- Gilbert CD, Sigman M (2007) Brain states: Top-down influences in sensory processing. *Neuron* 54:677–696.
- Schoups A, Vogels R, Qian N, Orban G (2001) Practising orientation identification improves orientation coding in V1 neurons. *Nature* 412:549–553.
- Raiguel S, Vogels R, Mysore SG, Orban GA (2006) Learning to see the difference specifically alters the most informative V4 neurons. *J Neurosci* 26:6589–6602.
- Schwartz S, Maquet P, Frith C (2002) Neural correlates of perceptual learning: a functional MRI study of visual texture discrimination. *Proc Natl Acad Sci USA* 99:17137–17142.
- Sigman M, et al. (2005) Top-down reorganization of activity in the visual pathway after learning a shape identification task. *Neuron* 46:823–835.
- Lewis CM, Baldassarre A, Committer G, Romani GL, Corbetta M (2009) Learning sculpts the spontaneous activity of the resting human brain. *Proc Natl Acad Sci USA* 106:17558–17563.
- Li W, Piëch V, Gilbert CD (2004) Perceptual learning and top-down influences in primary visual cortex. *Nat Neurosci* 7:651–657.
- Biswal B, Yetkin FZ, Haughton VM, Hyde JS (1995) Functional connectivity in the motor cortex of resting human brain using echo-planar MRI. *Magn Reson Med* 34:537–541.
- Fox MD, et al. (2005) The human brain is intrinsically organized into dynamic, anti-correlated functional networks. *Proc Natl Acad Sci USA* 102:9673–9678.
- Fox MD, Corbetta M, Snyder AZ, Vincent JL, Raichle ME (2006) Spontaneous neuronal activity distinguishes human dorsal and ventral attention systems. *Proc Natl Acad Sci USA* 103:10046–10051.
- Vincent JL, et al. (2006) Coherent spontaneous activity identifies a hippocampal-parietal memory network. *J Neurophysiol* 96:3517–3531.
- Greicius MD, Krasnow B, Reiss AL, Menon V (2003) Functional connectivity in the resting brain: a network analysis of the default mode hypothesis. *Proc Natl Acad Sci USA* 100:253–258.
- Hampson M, Driesen NR, Skudlarski P, Gore JC, Constable RT (2006) Brain connectivity related to working memory performance. *J Neurosci* 26:13338–13343.
- Seeley WW, et al. (2007) Dissociable intrinsic connectivity networks for salience processing and executive control. *J Neurosci* 27:2349–2356.
- van den Heuvel MP, Stam CJ, Kahn RS, Hulshoff Pol HE (2009) Efficiency of functional brain networks and intellectual performance. *J Neurosci* 29:7619–7624.
- Koyama MS, et al. (2011) Resting-state functional connectivity indexes reading competence in children and adults. *J Neurosci* 31:8617–8624.
- Zhu Q, Zhang J, Luo YL, Dilks DD, Liu J (2011) Resting-state neural activity across face-selective cortical regions is behaviorally relevant. *J Neurosci* 31:10323–10330.
- Sigman M, Gilbert CD (2000) Learning to find a shape. *Nat Neurosci* 3:264–269.
- Abdi H, Valentin D (2007) Multiple factor analysis (MFA). *Encyclopedia of Measurement and Statistics*, ed Salkind N (Sage Publications, Thousand Oaks, CA).
- Van Essen DC (2005) A Population-Average, Landmark- and Surface-based (PALS) atlas of human cerebral cortex. *Neuroimage* 28:635–662.
- Dosenbach NU, et al. (2006) A core system for the implementation of task sets. *Neuron* 50:799–812.
- Dosenbach NU, et al. (2007) Distinct brain networks for adaptive and stable task control in humans. *Proc Natl Acad Sci USA* 104:11073–11078.
- Shulman GL, et al. (1997) Common blood flow changes across visual tasks: II. Decreases in cerebral cortex. *J Cogn Neurosci* 9:648–663.
- Raichle ME, et al. (2001) A default mode of brain function. *Proc Natl Acad Sci USA* 98:676–682.
- Vincent JL, et al. (2007) Intrinsic functional architecture in the anaesthetized monkey brain. *Nature* 447:83–86.
- Stark DE, et al. (2008) Regional variation in interhemispheric coordination of intrinsic hemodynamic fluctuations. *J Neurosci* 28:13754–13764.
- Gál V, et al. (2009) Learning to filter out visual distractors. *Eur J Neurosci* 29:1723–1731.
- Bisley JW, Goldberg ME (2003) Neuronal activity in the lateral intraparietal area and spatial attention. *Science* 299:81–86.
- Sylvester CM, Shulman GL, Jack AI, Corbetta M (2007) Asymmetry of anticipatory activity in visual cortex predicts the locus of attention and perception. *J Neurosci* 27:14424–14433.
- Shulman GL, et al. (2003) Quantitative analysis of attention and detection signals during visual search. *J Neurophysiol* 90:3384–3397.
- Shulman GL, Astafiev SV, McAvoy MP, d'Avossa G, Corbetta M (2007) Right TPJ deactivation during visual search: Functional significance and support for a filter hypothesis. *Cereb Cortex* 17:2625–2633.
- Weissman DH, Woldorff MG (2005) Hemispheric asymmetries for different components of global/local attention occur in distinct temporo-parietal loci. *Cereb Cortex* 15:870–876.
- Honey CJ, et al. (2009) Predicting human resting-state functional connectivity from structural connectivity. *Proc Natl Acad Sci USA* 106:2035–2040.
- Ko H, et al. (2011) Functional specificity of local synaptic connections in neocortical networks. *Nature* 473:87–91.
- Johansen-Berg H (2007) Structural plasticity: Rewiring the brain. *Curr Biol* 17:R141–R144.
- Gattas R, Sousa AP, Mishkin M, Ungerleider LG (1997) Cortical projections of area V2 in the macaque. *Cereb Cortex* 7:110–129.
- Nir Y, et al. (2007) Coupling between neuronal firing rate, gamma LFP, and BOLD fMRI is related to interneuronal correlations. *Curr Biol* 17:1275–1285.
- He BJ, Snyder AZ, Zempel JM, Smyth MD, Raichle ME (2008) Electrophysiological correlates of the brain's intrinsic large-scale functional architecture. *Proc Natl Acad Sci USA* 105:16039–16044.
- de Pasquale F, et al. (2010) Temporal dynamics of spontaneous MEG activity in brain networks. *Proc Natl Acad Sci USA* 107:6040–6045.
- Buzsáki G, Draguhn A (2004) Neuronal oscillations in cortical networks. *Science* 304:1926–1929.
- Fries P (2005) A mechanism for cognitive dynamics: Neuronal communication through neuronal coherence. *Trends Cogn Sci* 9:474–480.
- Arieli A, Sterkin A, Grinvald A, Aertsen A (1996) Dynamics of ongoing activity: Explanation of the large variability in evoked cortical responses. *Science* 273:1868–1871.
- Kenet T, Bibitchkov D, Tsodyks M, Grinvald A, Arieli A (2003) Spontaneously emerging cortical representations of visual attributes. *Nature* 425:954–956.
- Sadaghiani S, Hesselmann G, Friston KJ, Kleinschmidt A (2010) The relation of ongoing brain activity, evoked neural responses, and cognition. *Front Syst Neurosci* 4:20.

# Supporting Information

Baldassarre et al. 10.1073/pnas.1113148109

## SI Methods

**Participants.** Fourteen healthy, right-handed volunteers (seven female; aged 20–30 y) with normal or corrected-to-normal vision participated in the study, after providing written informed consent approved by the institutional review board of the University “G. d’Annunzio” of Chieti, Italy. All subjects were screened for a history of psychiatric or neurological disorders, and were not taking any medications.

**Visual Stimuli.** The visual stimuli were generated using in-house software (LabScript) implemented in MATLAB (MathWorks). They were projected on a NEC 75 F Multisync monitor using a YASHI Pentium 4 computer during the behavioral training sessions, and back-projected to a translucent screen by an LCD video projector (830 G+; NEC), which was viewed through a mirror attached to the head coil during functional MRI (fMRI). The timing of stimulus presentation was synchronized to the acquisition of the fMRI frames.

The stimulus pattern was an annulus (5° radius) formed by 12 letter Ts (size, 1.5° visual angle) equally spaced and displayed randomly in four orientations (canonical, inverted 180°, and 90° rotated to the left or right). The target shape was always an inverted T, whereas Ts of different orientation were used as distracters.

**Behavioral Training.** During daily training sessions, participants were instructed to attend to the left lower visual quadrant and report the presence/absence of the target shape while maintaining central fixation (Fig. 1). The position of the eyes was monitored with an infrared eye tracker (ETL-400; iSCN). Each trial began with a central fixation spot followed by the presentation of the target shape for 2,000 ms, and then by the stimulus pattern for 150 ms. In the stimulus pattern, the target shape randomly appeared in one of three possible locations in the left lower visual quadrant, whereas the distracters, changing orientation randomly on each trial, were displayed in the remaining 11 locations across the four visual quadrants. Subjects indicated the presence/absence of the target shape by pressing one of two response keys on a Cedrus button box while maintaining fixation on the central spot. Participants performed blocks of 45 trials, of which 36 (80%) contained the target, and nine (20%) did not. In each daily session subjects ran, on average, approximately 30 blocks of trials (range, 10–45 blocks). Training was discontinued when each observer reached a criterion of greater than 80% accuracy in at least 10 consecutive blocks.

**fMRI Procedure and Scanning.** Before behavioral training, subjects were scanned on a 1.5-T Siemens Vision scanner to obtain anatomical and functional scans. Anatomical images were acquired with a sagittal magnetization-prepared rapid acquisition gradient echo T1-weighted sequence (MPRAGE) with repetition time of 9.7 s, echo time of 4 ms, flip angle of 12°, time for inversion of 1,200 ms, and voxel size of 1 × 1 × 1.25 mm. Functional images were acquired with a gradient-echo sequence (repetition time, 2.163 s; echo time, 50 ms; flip angle, 90°; slice thickness, 8 mm) in the axial plane (matrix, 64 × 64; field of view, 240 mm; 3.75 × 3.75 mm in-plane resolution). Sixteen slices were acquired for whole-brain coverage.

The fMRI data were acquired at rest, and during visuotopic localizer scans designed to identify regions in visual occipital cortex responding preferentially to the stimulus pattern in each of the four visual quadrants. During the resting-state scans, subjects were instructed to fixate a small cross in a low luminance envi-

ronment and remain passive. Six scans of resting state, each including 128 volumes, were acquired. During the localizer scans, subjects were asked to maintain central fixation and quarter-field stimuli were presented in a blocked design alternating with fixation periods (Fig. 1C). Each scan consisted of 20 blocks: 16 stimulation blocks (four for each visual quadrant: left lower, right lower, left upper, and right upper), in which an array of three letter Ts was flashed at 6.67 Hz for 13 s, and four fixation blocks that were randomly interspersed among the stimulation blocks. Six runs of visuotopic localizer scans, each including 117 volumes, were obtained.

A second scanning session was performed after the perceptual training was completed to define brain regions recruited by the task. In a blocked design, subjects performed the orientation task by using the familiar shape used for training (inverted letter T) or a novel shape (a T rotated 90° to the left or right). In both conditions, the target was always randomly presented at one of the three locations of the stimulus array in the trained quadrant. The two tasks were run in blocks of trials beginning with a central cue (duration, 2.163 s) indicating the upcoming target (duration, 2.163 s), with each block lasting for 12 s (six trials per block). The target was present on 80% of the trials, as in the behavioral session. Fixation blocks of 6, 10, or 12 s, with equal probability, were randomly interspersed with the active task blocks. Six scans, each including 113 volumes, were obtained, equal to 18 blocks (or 108 trials) per condition.

**Behavioral Analysis.** Percent accuracy was computed for each block of training as follows (1, 2):

$$\frac{[\text{hits} (\%) + \text{correct rejections} (\%)] - \text{false alarms} (\%)}{1 - \text{false alarms} (\%)} \quad \text{[S1]}$$

Individual raw learning curves were smoothed by using a five-point moving average (MATLAB; MathWorks), and were fit with a model fit using an empirical two-parameter expression:

$$a = a_0 + s \log(k) \quad \text{[S2]}$$

where  $a$  is accuracy,  $k$  indexes block,  $a_0$  is initial accuracy on the first block, and  $s$  is a scaling parameter numerically equal to the initial slope, by using Curve Fitting Toolbox 2.0 (MATLAB; MathWorks). This model provided the best fit of the psychophysical performance curves, compared with linear and sigmoidal fits, expressed in terms of variance explained ( $r^2$ ): median  $r^2$  of 0.68, range of 0.29–0.93 (Fig. 1B and Fig. S1). In addition to  $a_0$  and  $s$ , the number blocks needed to achieve criterion (i.e., 80% performance,  $k_c$ , was evaluated (Fig. S2A shows individual scores). These three measures were correlated: initial accuracy and slope ( $r = -0.85$ ;  $P < 0.001$ ), initial accuracy and blocks to criterion ( $r = -0.68$ ;  $P < 0.01$ ), and slope and blocks to criterion ( $r = 0.27$ ;  $P < 0.3$ ; Fig. S2). After normalizing the behavioral parameters (mean = 0, SD = 1), we attempted to reduce the dimensionality by computing a principal component analysis (PCA).

To obtain individual quantitative indices of performance,  $a_0$ ,  $s$ , and  $k_c$  were entered into a PCA (Fig. S3). The first component (i.e., PC1) explained 75% of the variance. The second component accounted for 15% of the variance, but its eigenvalue was less than 1 (scree plot in Fig. S3) and it was therefore not further considered (3). Accordingly, PC1 was used to compute individual measures of performance, which we here define as “task fitness”, using the following expression:

$$f = [a_0 \ s \ k_c] \cdot w \quad [\text{S3}]$$

where  $w$  is the vector of factor weights (0.6619,  $-0.5655$ , and  $-0.4920$ ) for initial accuracy  $a_0$ , slope  $s$ , and number of blocks to criterion  $k_c$ , respectively. The first component represents a predictor of our observers' fitness or aptitude toward performing the orientation discrimination task. Principal component scores for PC1 from each subject were used as regressors for all of the functional connectivity (FC) and behavior correlation analysis (Fig. S3B).

**fMRI Data Preprocessing.** Functional data were realigned within and across scanning runs to correct for head motion by using an eight-parameter (rigid body plus in-plane stretch) cross-modal registration. Differences in the acquisition time of each slice within a frame were compensated for by sync interpolation. A whole-brain normalization factor was applied to each run to correct for changes in signal intensity between runs (mode of 1,000). For each subject, an atlas transformation (4) was computed on the basis of an average of the first frame of each functional run and MPRAGE structural images to the atlas representative target by using a 12-parameter general affine transformation. Functional data were interpolated to 3-mm cubic voxels in atlas space. The atlas representative MPRAGE target brain (711–2C) was produced by mutual coregistration (12 parameters affine transformations) of images obtained in 12 normal subjects (4). All preprocessing steps were performed by using in-house software.

**Visuotopic Localizer and Orientation Discrimination Task Data Processing.** The blood oxygenation level-dependent (BOLD) time course at each voxel, for each subject, was subjected to a general linear model with an assumed response function (Boynton hemodynamic model) (5) by using in-house software. Constant and linear terms over each BOLD run accounted for baseline and linear drift. Separate task regressors coded for each of the event types [five for the visuotopic localizer (fixation, left lower quadrant, right lower quadrant, left upper quadrant, and right upper quadrant); three for the orientation discrimination task (fixation, trained shape, untrained shape)]. A “residuals” dataset was created by summing the modeled responses (but not the constant or linear drift) with the residuals unaccounted for by the linear model. Therefore, this dataset contains the original time series minus the constant and linear drift terms. Group analyses were conducted using voxel-wise random-effect ANOVAs. Statistical images were Monte Carlo corrected for multiple comparisons over the entire brain ( $P < 0.05$ ) to obtain Z-score maps. Contrast maps were computed by subtracting ANOVA effects at each voxel to create Z-score images from a given GLM. For the visuotopic localizer, voxels responding preferentially to each visual quadrant were found by contrasting the Z-score image for the desired visual quadrant with the average of the Z-score images from the other quadrants.

**Additional Preprocessing for Resting-State Data.** In preparation for the FC MRI analysis, data were passed through several additional preprocessing steps (6): (i) spatial smoothing (6 mm full width at half maximum Gaussian blur), (ii) temporal filtering retaining frequencies in the 0.009–0.08 Hz band, and (iii) removal of the following sources of spurious variance unlikely to reflect spatially specific functional correlations through linear regression: (i) six parameters obtained by rigid body correction of head motion, (ii) the whole-brain signal averaged over a fixed region in atlas space, (iii) signal from a ventricular region of interest (ROI), and (iv) signal from a region centered in the white matter.

**Seed Regions.** A set of seed regions in visual cortex, and auditory cortex was functionally defined from localizer and task contrast

maps by using an in-house clustering algorithm. Seeds were initially defined as 15-mm spheres centered on peaks (threshold between Z-score 3 and  $-3$ ); peaks within 15 mm of each other were consolidated into a single ROI. Stimulus-specific seeds in visual cortex were defined on the basis of localizer contrast maps: desired quadrant vs. average of all other quadrants. For each quadrant, the two strongest responses were selected. Their location was defined based on their overlap with the probabilistic borders of retinotopic areas in the Population Average Landmark and Surface (PALS) atlas (7), similarly to our previous study (8). In general, for each quadrant, we obtained a response in early visual cortex (i.e., V1/V2) and one in intermediate visual cortex (i.e., V3–VP/V4–V3A). Moreover, a set of control regions in auditory cortex was defined from the task activation data by using the contrast Trained plus Untrained shape vs. Fixation. During a visual task, strong deactivations are typically observed in auditory cortex (9). Accordingly, two primary and two secondary auditory regions were selected in each hemisphere for the FC analysis. All the seeds are listed in Table S1.

**Resting-State FC Over Whole Brain.** In each participant, voxel-wise resting state FC maps were computed for each seed (e.g., right dorsal V1–V2) by extracting time course from a given seed and then computing the correlation coefficient (Pearson  $r$ ) between that time course and the time course from all other brain voxels. Correlation coefficients were converted to a normal distribution by Fisher Z-transform.

**FC-Behavior Correlation Over Whole Brain.** For each of the eight visual ROIs, we computed voxel-wise correlation maps between behavior and FC, i.e., FC–PC1 correlation maps, by using individual factor scores of the first component (i.e., PC1) of the behavioral PCA (Fig. S4). These maps were computed by calculating at each voxel the correlation coefficient (Pearson correlation coefficient  $r$ ) between FC for a seed region (e.g., right dorsal V1–V3) and the rest of the brain, and behavioral scores over the group of subjects. Considering  $x$  equal to behavioral score (e.g., factor score of PC1) and  $y$  equal to FC between a visual seed region (e.g., right dorsal V1–V3) and a given voxel, we used the following formula:

$$r = \frac{1}{n-1} \sum_{i=1}^n \left[ \left( \frac{X_i - \bar{X}}{\sigma_X} \right) \left( \frac{Y_i - \bar{Y}}{\sigma_Y} \right) \right] \quad [\text{S4}]$$

where  $n$  is the number of subjects (14);  $X_i$ ,  $\bar{X}$ , and  $\sigma_X$  are the score, sample mean, and sample SD for the behavior respectively; and  $Y_i$ ,  $\bar{Y}$ , and  $\sigma_Y$  are the score, sample mean, and sample SD for the FC, respectively.

This computation generated a voxel-wise correlation map indicating which voxels showed a significant association (positive or negative correlation) between FC with a given visual seed region (right dorsal V1–V3) and the behavioral score (Fig. S4 shows analysis flowchart). The  $r$ -score maps were transformed first into  $t$ -score and then to Z-statistic maps. The final Z-statistic maps were corrected for Monte Carlo multiple comparisons ( $Z > 2$ ,  $P < 0.05$ ; Fig. S5). These maps are defined as FC–PC1 correlation maps.

The consistency of the topography of the behaviorally significant FC was quantified by a conjunction analysis of thresholded FC–PC1 maps across seed regions. A positive value in a given voxel indicates how many visual seeds show positive correlation between behavioral score and its FC with that voxel. At the same time, a negative value indicates how many seeds exhibit negative correlations. Given that we used eight visual seeds (Fig. 1D), the maximum value in the conjunction maps was  $\pm 8$ . The same procedure was performed for the four control regions in the auditory cortex.

**FC-Behavior vs. Task-Evoked Topography.** The overlap of regions showing positive FC–PC1 correlation with those responding during the visuotopic localizer or the task was quantified by computing the percentage of voxels overlapping between FC–PC1 correlation conjunction maps, and sum maps of task-evoked activity. For the visuotopic condition, the four quadrant-related Z-score (multiple comparisons corrected) maps were summed. The sum map was thresholded at a  $Z$  of 3 and transformed to a binary map (Fig. 2D). For the orientation task, Z-maps with positive or negative modulation above a  $Z$  value threshold  $\pm 3$  for the contrast trained plus untrained vs. fixation were summed. Percentage of voxel overlap between FC–PC1 correlation conjunction and sum maps of task-evoked activity were calculated at different conjunction thresholds (e.g., four of eight seeds, six of eight seeds).

**FC-Behavior Correlation at the Regional Level.** In addition to computing the FC–behavior correlation over the whole brain, we also conducted FC–PC1 correlation analyses at the regional level. BOLD time series were extracted from visuotopic ROIs (Table S1; Seed ROIs), and correlation matrix was created by computing the pairwise temporal correlation (Pearson correlation coefficient  $r$ ) across all ROIs. This  $r$ -score matrix was then converted by Fisher  $Z$ -transform into a normalized  $Z$ -score matrix (Fig. 3A). Finally, the  $Z$ -score FC matrix was correlated across subjects with the PC1 scores (Fig. 3B). A correction for multiple comparisons was implemented by a random permutation test, and thresholded at a false discovery rate of  $q < 0.05$  for 1,000 permutations.

1. Sigman M, Gilbert CD (2000) Learning to find a shape. *Nat Neurosci* 3:264–269.
2. Sigman M, et al. (2005) Top-down reorganization of activity in the visual pathway after learning a shape identification task. *Neuron* 46:823–835.
3. Abdi H, Valentin D (2007) Multiple factor analysis (MFA). *Encyclopedia of measurement and statistics*, ed Salkind N (Sage, Thousand Oaks, CA).
4. Snyder AZ (1995) Difference image vs ratio image error function forms in PET-PET realignment in quantification of brain function using PET. *Quantification of Brain Function Using PET*, eds Myer R, Cunningham VJ, Bailey DL, Jones T (Academic, San Diego), pp 131–137.
5. Boynton GM, Engel SA, Glover GH, Heeger DJ (1996) Linear systems analysis of functional magnetic resonance imaging in human V1. *J Neurosci* 16:4207–4221.
6. Fox MD, et al. (2005) The human brain is intrinsically organized into dynamic, anticorrelated functional networks. *Proc Natl Acad Sci USA* 102:9673–9678.
7. Van Essen DC (2005) A Population-Average, Landmark- and Surface-based (PALS) atlas of human cerebral cortex. *Neuroimage* 28:635–662.
8. Lewis CM, Baldassarre A, Committeri G, Romani GL, Corbetta M (2009) Learning sculpts the spontaneous activity of the resting human brain. *Proc Natl Acad Sci USA* 106:17558–17563.
9. Shulman GL, et al. (1997) *J Cogn Neurosci* 9:648–663.

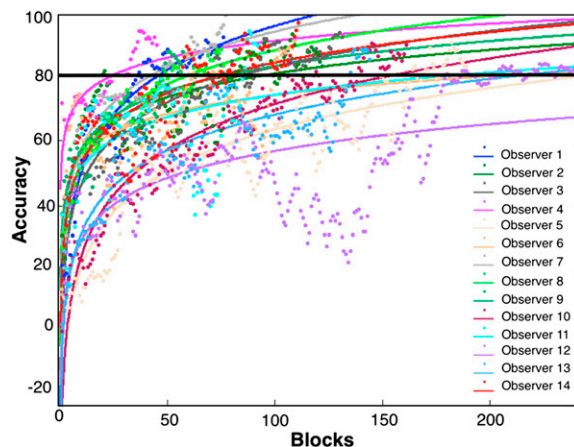


**Fig. S1.** Individual learning curves and logarithmic fit. x axis, progressive number of blocks; y axis, accuracy (percentage of correct response corrected for false alarms (Eq. S1)). Dots indicate individual blocks and lines indicate individual logarithmic fit curves. Each color refers to a single observer.



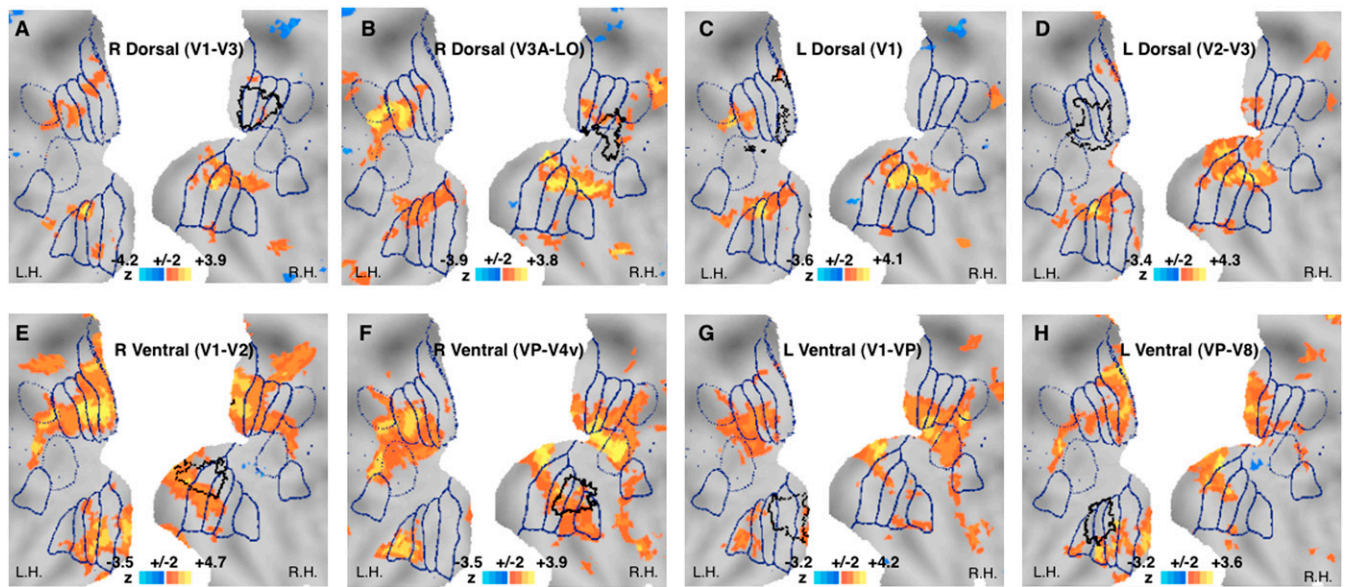


**Fig. 55.** FC by task fitness (PC1) correlation maps in visual cortex. Voxel-wise FC-PC1 correlation maps projected onto a flattened representation of the posterior occipital cortex using the PALS atlas (1). Each map (A-H) corresponds to FC to/from a separate stimulus region (black borders) independently defined from the visuotopic localizer scans: Right dorsal V1-V3 (A), right dorsal V3A-LO (B), left dorsal V1 (C), left dorsal V2-V3 (D), right ventral V1-V2 (E), right ventral VP-V4v (F), left ventral V1-VP (G), and left ventral VP-V8 (H). Color scale: yellow/orange indicates positive correlation (Z-statistic of Pearson  $r$ ) thresholded at  $Z > 2$ ,  $P < 0.05$ , and Monte Carlo corrected. Blue color indicates negative correlation. Blue lines define population average retinotopic borders in the PALS atlas (1). L.H., left hemisphere; R.H., right hemisphere.

1. Van Essen DC (2005) A population-average, landmark- and surface-based (PALS) atlas of human cerebral cortex. *Neuroimage* 28:635-662.

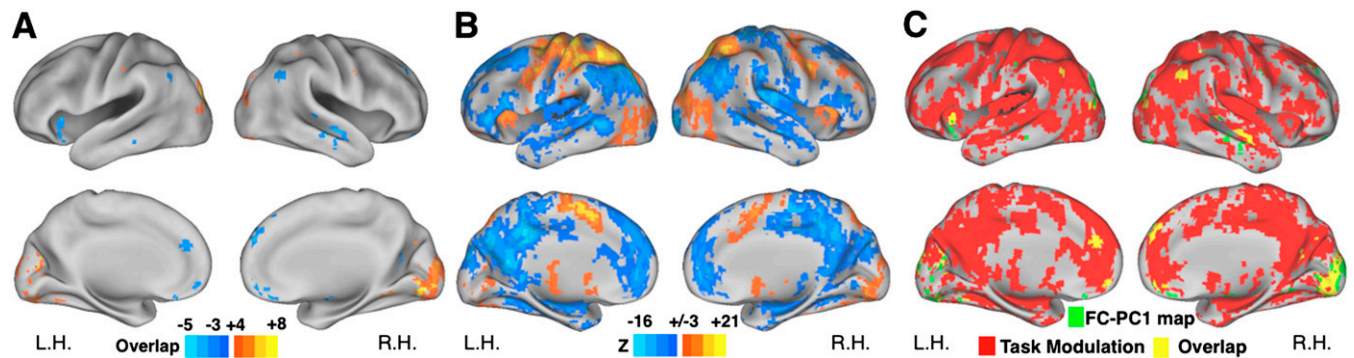


**Fig. 56.** Predictive intrinsic FC and task activations. (A) Voxel-wise of the conjunction map of eight FC-PC1 correlation maps, one for each visual seed shown in Fig. 1D (Table S1 shows coordinates). Color scale: yellow/red indicates overlap of positive correlations (range, 1-8); cyan/blue indicates overlap of negative correlation. (B) Voxel-wise activation map for visual orientation task (trained plus untrained shape minus fixation conditions). Color scale: Z-statistic  $> 3$ ,  $P < 0.05$ , Monte Carlo corrected. Yellow/red, activation; cyan/blue, deactivation. (C) Conjunction map between FC-PC1 conjunction map (A), thresholded at positive four of eight and at negative three of eight (green) and activation map of orientation discrimination task (B) (red). Overlapped voxels are in yellow.

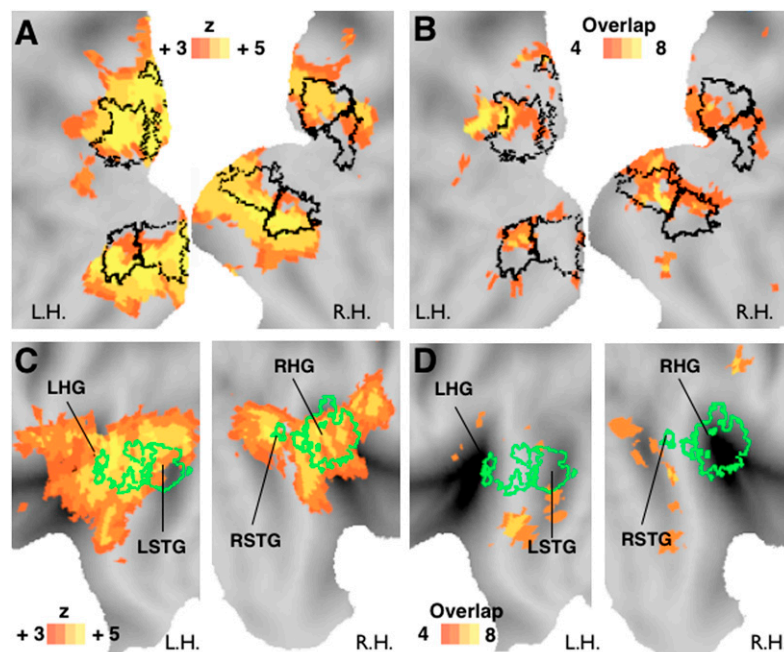


**Fig. S7.** Task fitness and FC: visual vs. auditory. (A) Average FC map obtained by averaging individual maps from our eight stimulus seed ROIs in visual cortex (black borders; same as Fig. S5). Color scale: yellow/orange indicates voxels showing positive FC (Z-statistic of Pearson  $r$ , thresholded at  $Z > 3$ ,  $P < 0.05$ , Monte Carlo corrected). (B) Conjunction of eight voxel-wise FC–PC1 correlation maps, one for each visual seed (Table S1 includes coordinates). Yellow/red indicates overlap of positive correlations (range, 1–8). (C) Average FC map obtained by averaging individual FC maps obtained from four auditory seed ROIs (green borders). The ROIs in auditory cortex were obtained by selecting negative (i.e., deactivation) responses during performance of the visual orientation discrimination task in Heschl gyrus and superior temporal gyrus corresponding to primary and secondary auditory cortices. The map is projected on the flattened representation of the right (*Right*) and left (*Left*) temporal lobes by using the PALS atlas (1). Color scale is the same as in A. (D) Conjunction map of four FC–PC1 correlation maps, one for each auditory seed (Table S1 shows coordinates). Color scale is the same as in B. LHG, left Heschl gyrus; LSTG, left superior temporal gyrus; RHG, right Heschl gyrus; RSTG, right superior temporal gyrus.

1. Van Essen DC (2005) A population-average, landmark- and surface-based (PALS) atlas of human cerebral cortex. *Neuroimage* 28:635–662.

**Table S1. Seed ROIs**

Coordinates	Regions	Label	Network	Origin	Voxels	Z-score
+14 –92 +20	Right early dorsal visual cortex	Right dorsal V1–V3	Visual	Visuotopic	221	25.35
+28 –86 +11	Right intermediate dorsal visual cortex	Right dorsal V3A–LO	Visual	Visuotopic	138	16.04
–13 –97 +14	Left early dorsal visual cortex	Left dorsal V1	Visual	Visuotopic	104	19.26
–10 –85 +1	Left intermediate dorsal visual cortex	Left dorsal V2–V3	Visual	Visuotopic	220	12.73
+9 –80 –6	Right early ventral visual cortex	Right ventral V1–V2	Visual	Visuotopic	201	28.94
+23 –75 –12	Right intermediate ventral visual cortex	Right ventral VP–V4	Visual	Visuotopic	249	17.70
–19 –78 –12	Left early ventral visual cortex	Left ventral V1–VP	Visual	Visuotopic	214	23.05
–4 –83 –7	Left intermediate ventral visual cortex	Left ventral VP–V8	Visual	Visuotopic	163	18.65
+41 –26 +17	Right Heschl gyrus	Right HG	Auditory	Task	282	–11.90
+63 –27 +14	Right superior temporal gyrus	Right STG	Auditory	Task	54	–6.00
–45 –36 +2	Left Heschl gyrus	Left HG	Auditory	Task	114	–8.50
–62 –35 +7	Left superior temporal gyrus	Left STG	Auditory	Task	117	–8.60

List of ROIs. Coordinates, [x, y, z] according to Talairach atlas (1) used for FC analysis. Origin, contrasts from which ROIs were selected; Visuotopic, stimulus localizer; Task, subtraction between task Trained + Untrained vs. Fixation.

1. Talairach J, Tournoux P (1998) *Co-Planar Stereotaxic Atlas of the Human Brain* (Thieme Medical Publishers, New York).

**Table S2. Regions with behaviorally significant FC from visual areas**

Region	Overlap	Seeds	Correlation
R VP	8/8	All	Positive
R VP	7/8	All except R ventral V1–V2	Positive
R V2v	7/8	All except R ventral V1–V2	Positive
L V3A	7/8	All except L dorsal V1	Positive
L V7	7/8	All except L dorsal V1	Positive
R V2d	6/8	All except R dorsal V1–V3, L dorsal V1	Positive
R V3–V3A	6/8	All except L dorsal V1, L dorsal V2–V3	Positive
R V1v	6/8	All except R dorsal V3A–LO, L dorsal V1	Positive
R V2v	6/8	All except R dorsal V3A–LO, L dorsal V1	Positive
R V4v	6/8	All except L dorsal V1, R ventral V1–V2	Positive
L V1d	6/8	All except R dorsal V3A–LO, R ventral VP–V4	Positive
L V3	6/8	All except L dorsal V1, L dorsal V2–V3	Positive
L V3A	6/8	All except L dorsal V1, L dorsal V2–V3	Positive
L V4v	6/8	All except R ventral V1–V2, L ventral VP–V8	Positive
R V1d	5/8	L V2–V3d, R V1–V2v, R VP–V4v, L V1–VPv, L VP–V8v	Positive
R V2d	5/8	R V3A–LOd, R V1–V2v, R VP–V4v, L V1–VPv, L VP–V8v	Positive
R V3	5/8	R V3A–LOd, R V1–V2v, R VP–V4v, L V1–VPv, L VP–V8v	Positive
R V3A	5/8	R V3A–LOd, R V1–V2v, R VP–V4v, L V1–VPv, L VP–V8v	Positive
R V1v	5/8	L V2–V3d, R V1–V2v, R VP–V4v, L V1–VPv, L VP–V8v	Positive
R VP	5/8	R V1–V3d, R V3A–LOd, R V1–V2v, L V1d, L V2–V3d	Positive
R V4v	5/8	R V1–V2v, R VP–V4v, L V1–VPv, L VP–V8v, L V1d	Positive
L V1d	5/8	R V1–V3d, R V1–V2v, L V2–V3d, R V1–V2v, L V1d	Positive
L V3A	5/8	R V1–V3d, R V3A–LOd, R V1–V2v, R VP–V4v, L V1d	Positive
L V7	5/8	R V1–V3d, R V3A–LOd, R V1–V2v, R VP–V4v, L V1d	Positive
L VP	5/8	R V1–V3d, R V3A–LOd, R V1–V2v, L V2–V3d, L V1d	Positive
L V4v	5/8	R V1–V3d, R V3A–LOd, R V1–V2v, L VP–V8v, L V1d	Positive
R STS	5/8	R V1–V3d, R V3A–LOd, R V1–V2v, L VP–V8v, L V1d	Negative
R MFG	5/8	R V1–V3d, R V3A–LOd, R V1–V2v, L VP–V8v, L V1d	Negative
R mvPFC	4/8	L V2–V3d, R V1–V2v, L V1–VPv, L VP–V8v	Negative
R mdPFC	4/8	L V2–V3d, R V1–V2v, L V1–VPv, L VP–V8v	Negative
L mvPFC	4/8	R V1–V2v, R VP–V4v, L V1–VPv, L VP–V8v	Negative
L al	4/8	R V1–V3d, R V3A–LOd, R VP–V4v, L V1d	Negative
R AG	3/8	R V1–V3d, R V3A–LOd, L V1d	Negative
L mdPFC	3/8	R V1–V3d, R V3A–LOd, L V1d	Negative
L AG	3/8	R V1–V3d, R V3A–LOd, L V2–V3d	Negative

Regions, foci with significant FC-PC1 correlation; coordinates, *x*, *y*, *z*; overlap, number of visual ROIs with significant FC to this region (maximum *n* = 8 ROIs); correlation, direction (positive/negative) of FC-PC1 correlations. L, left; R, right; STS, superior temporal sulcus; MFG, middle frontal gyrus; mvPFC, medio-ventral prefrontal cortex; mdPFC, medio-dorsal prefrontal cortex; al, anterior insula; AG, angular gyrus.